Performance of Buttress Wall in a Deep Excavation in Soft Ground

L.W. Wong

SMEC Asia Limited, Hong Kong

doi: https://doi.org/10.21467/proceedings.159.8

ABSTRACT

Diaphragm wall strengthened with buttress panels has frequently been adopted for reducing the wall deflections and the adjacent ground surface settlements caused by deep excavations. A case history on top-down construction with the excavation depth of 32 m is reviewed to study the effect of the buttresses on reduction in wall deflections. The excavation was supported by perimeter diaphragm walls of 1.5 m in thickness, 52 m in length and stiffened with buttresses spacing at 8.75 m. Two-Dimensional numerical analyses using the nonlinear Hardening-Soil with Small-Strain Stiffness constitutive soil model have been conducted. Five sets of wall stiffnesses with different interface reduction factors have been adopted to simulate buttresses with various spacing. Close matching between the computed wall deflections with those observed in the inclinometers validated the set of the soil stiffness parameters for the Hardening-Soil with Small-Strain Stiffness model. The effectiveness of the buttresses was assessed by comparing the computed wall deflections with and without the buttress panels.

Keywords: Excavation, Hardening Soil Model, Small Strain, Buttress, Ground Movements

1 Introduction

Ground movements caused by deep excavations have been one of the prime concerns for underground construction in urban areas. In order to minimize their adverse effects to structures nearby, strengthening measures have often been constructed in addition to the perimeter diaphragm walls. The use of jet grout slabs, cross-walls and buttress walls as the strengthening measures have been reported in the literature. Chuang *et al.* (2002) reported the use of buttresses to reduce the diaphragm wall deflections for a 32 m deep excavation. Ou *et al.*, (2006) presented case records on excavation with cross-walls and buttresses in basement excavations.

In order to study the effectiveness of buttress walls in reducing ground movements, performance of the diaphragm wall strengthening with buttresses for a case history is critically reviewed. The case of Core Pacific City Shopping Complex (CPC) was previously reported by Chuang *et al.* (2002) and Hwang *et al.*, (2007). As shown in Figures 1, the development comprised a 12-storey building complex and an 11-storey spherical shopping mall. The basement area was approximately 118 m along the north-south and the east-west directions as depicted in Figure 2. Excavation to a maximum depth of 31.7 m was carried out by using the top-down method of construction. The pit was retained by perimeter diaphragm walls and braced by floor slabs. Buttress panels were installed to reinforce the diaphragm walls at locations where there were existing buildings as a building protection measure.

Back-analyses have been conducted to evaluate the performance of the excavation by using the finite element computer code PLAXIS. The Hardening-Soil with small-strain Stiffness model (HSS), developed by Benz Thomas (2006) and introduced in the PLAXIS program (PLAXIS 2013), has been adopted to simulate the stress-strain-strength relationship of soils. Readings of inclinometers are available to compare with the results of the analyses. By matching the calculated wall deflection profiles with those observed, the soil parameters are validated. The effectiveness of buttresses in reducing wall deflections is assessed.

Proceedings DOI: 10.21467/proceedings.159; Series: AIJR Proceedings; ISSN: 2582-3922; ISBN: 978-81-965621-6-8

2 Subsoil Conditions

2.1 Ground conditions

The project site for Core Pacific City is located in the K1 Zone (MAA 1987; Lee 1996) in the southeast part of the Taipei Basin. As depicted in Figure 3, at the surface lies the Songshan Formation which typically comprises six alternating sand and clay layers. At the ascending order Sublayers I, III and V are sandy soil (SM) and Sublayers II, IV and VI are clayey soil (CL) strata. The underlying Jingmei Formation, a gravelly soil (GM) stratum, is encountered at the depth about 49 m (Elevation -43.5 m). The ground levels range from El. 5.5 m to El. 6.1 m above the mean sea level. Table 1 summarized the soil parameters for the various sublayers. At this site, the Songshan Formation is dominant with the thick clayey Sublayer IV and Sublayer II, which are encountered at the depths between 8 m and 32 m and between 34 m and 47 m respectively. The sandy Sublayers V, III and I are encountered at the depths of 4 m, 32 m and at 47 m respectively.

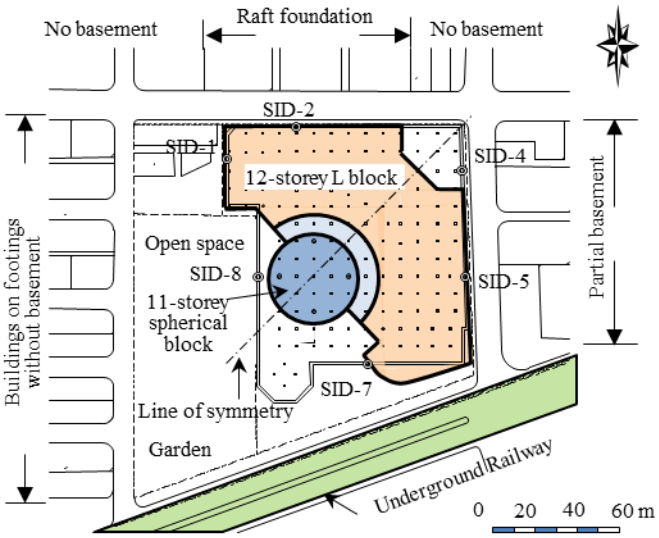

(a) Layout plan

(b) Isometric View

Figure 1: *General layout of Core Pacific City Shopping Complex (CPC)*

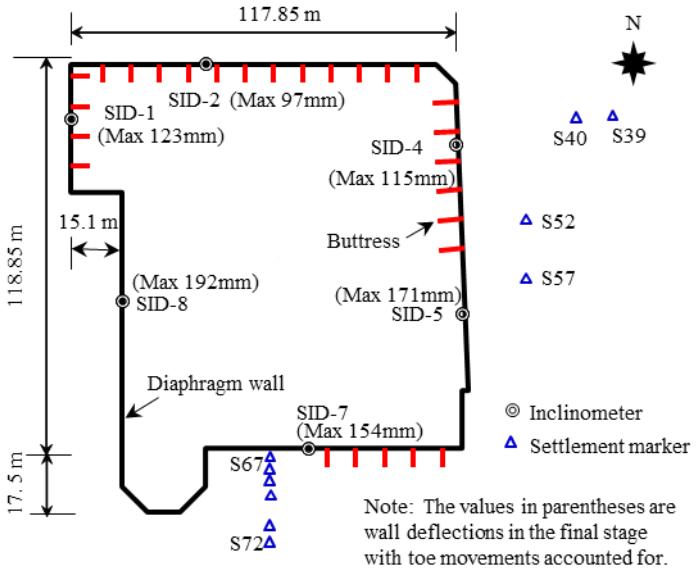

Figure 2: *Layout of diaphragm wall and buttress wall (after Hwang et al., (2007))*

A representative excavation model is shown in Figure 3. The excavation was carried out to a depth of 31.7 m in 9 stages. The pit was retained by diaphragm walls of 1.5 m in thickness and 52 m in length. Excavation for the foundation was constructed by the top-down method. The diaphragm wall was abutted by buttress panels of 1.5 m in thickness, 3.5 m to 3.7 m in breadth, 29.5 m in length and spacing at 8.75 m. The buttresses were installed and cast together with the diaphragm walls with reinforcement interlocked.

The excavation was conducted by top-down construction using the ground floor slab (GF) and 6 levels of basement floor slabs (B1 to B6) of 150 mm in thickness as the lateral supports. Temporary steel struts were erected at the openings at GF, B1 and B2 slabs. Excavation commenced in January 1999 and the foundation slab was cast in October 2000.

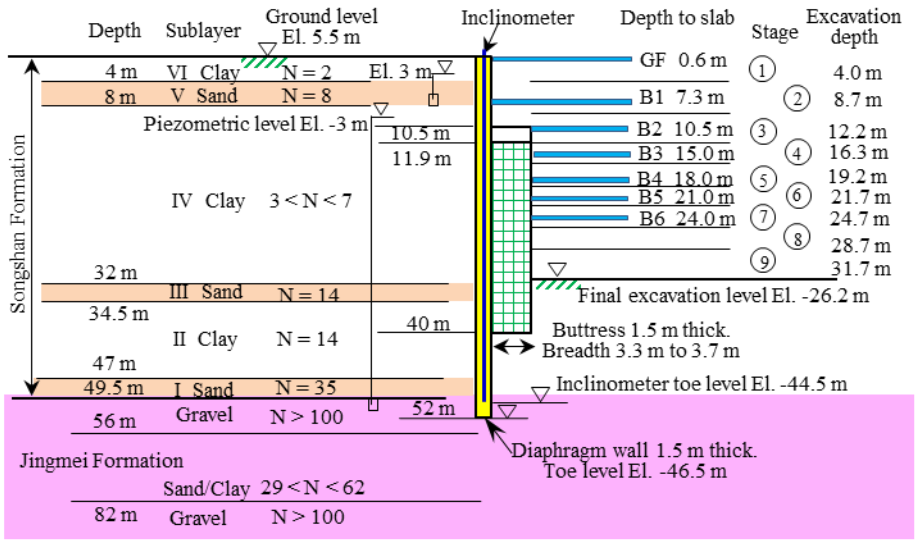

Figure 3: *Soil profile of the CPC Case and excavation scheme*

Proceedings DOI: 10.21467/proceedings.159
ISBN: 978-81-965621-6-8

Series: AIJR Proceedings
ISSN: 2582-3922

2.2 Undrained shear strengths

The properties of the six sublayers in the Songshan Formation have been well discussed in the literature (MOH & OU, 1979; MAA 1987). An advanced study was conducted by Geotechnical Engineering Specialty Consultant engaged by the Department of Rapid Transit Systems of Taipei City Government in the very early stage of the metro construction as a Designated Task to study the characteristics of Taipei clays (Chin *et al.*, 1994, 2007; Chin & Liu 1997; Hu. I.C. *et al.*, 1996). It was conducted in collaboration with a research team from Massachusetts Institute of Technology (MIT). Figure 4 presents the results of the CK_0UC tests conducted on the specimens recovered from borehole R-1 that Chin *et al.*, (1994) reported. Borehole R-1 was located in the K1 Geological Zone in Taipei Basin.

Kung *et al.* (2009) presented the results of undrained shear strength, s_u, for an excavation case history located at 300 m north of the CPC project site. The s_u values were determined from consolidated triaxial undrained compression tests conducted on specimens recovered from the clayey Sublayer IV. The specimens were saturated and K_0-consolidated to the in-situ effective stress states. The variation in undrained shear strengths for the compression tests that Ou *et al.* (2000) and Kung *et al.* (2009) reported are presented in Figure 4. Compared with the CK_0UC tests reported by Chin *et al.*, (1994), the s_u values obtained by Ou *et al.* (2000) and Kung *et al.* (2009) are lower, which would be attributable to sampling disturbance. Although the specimens were consolidated to the in-situ horizontal stress, such process could not fully compensate the effect due to sample disturbance. Based on the s_u profile presented in Figure 4, the s_u values varying from 50 kPa to 60 kPa can be obtained above a depth of 15 m. The Author has proposed in this study that the s_u values for the clay below 15 m depth can be expressed as follows:

$$s_u = 60 + 4.8\ (D\text{-}15) \quad (1)$$

where D is the depth in metre and s_u is the undrained shear strength in kPa.

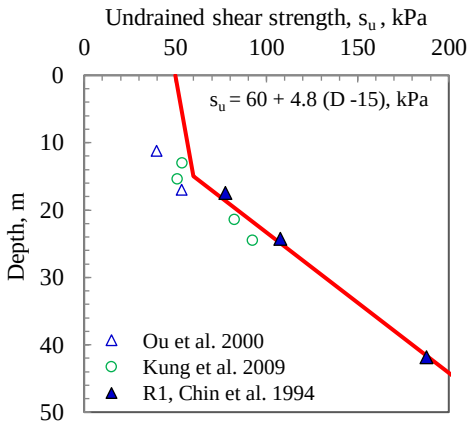

Figure 4: *Undrained shear strengths of clays obtained by CK_0UC triaxial tests*

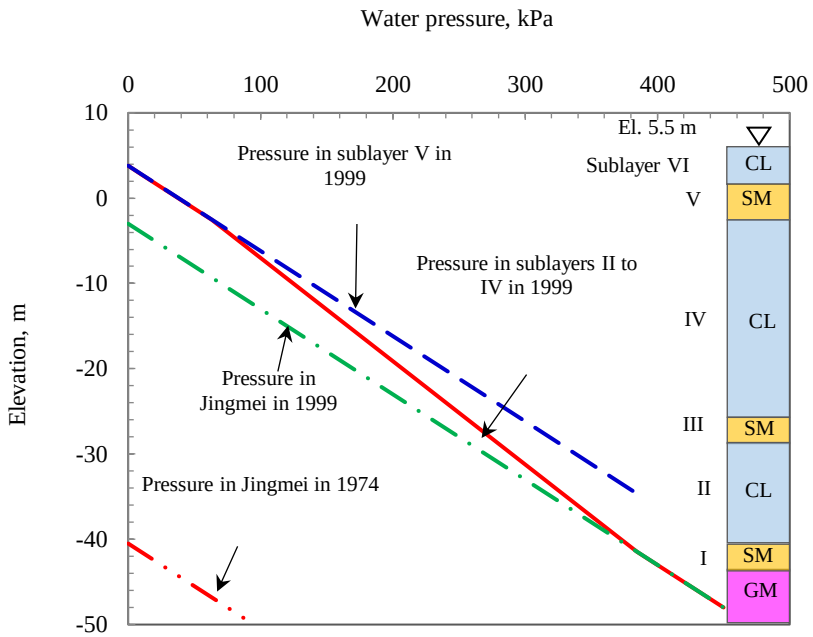

Figure 5: *Groundwater pressures on the outer face of the diaphragm walls*

2.3 Groundwater conditions

Piezometers monitoring was conducted prior to and during excavation for the CPC project site. The groundwater level in the Sublayer V sand was around El. 3 m. Due to excessive extraction of groundwater to supply water to the city, the piezometric levels in the Jingmei Formation were lowered to a level near the bottom of the Songshan Formation in the 1970s, leading to significant reductions in water pressures in the Songshan Formation and substantial ground settlements as a result. The piezometric levels in the Jingmei Formation did not recover till 1974 although pumping had been banned since 1968. The subsoils in the Songshan Formation in the Taipei Basin are thus substantially over-consolidated. This is particularly true for the clayey Sublayer II because the underlying sandy Sublayer I is so permeable that the piezometric levels in Sublayer I essentially dropped by the same magnitudes as those in the Jingmei Formation.

Based on monitoring records at the deep well at Sun Yet Sin Memorial Hall, located at 1 km south of the CPC project site, Hwang and Moh (2022) reported that the piezometric level in the Jingmei Formation in the eastern portion of the Taipei Basin was around El. -3 m in 1999. In the central portion of the Taipei Basin, the piezometric level in Jingmei Formation recovered to El. 0 m in 2017. The distributions of the water pressures outside the diaphragm wall at CPC in 1999 are presented in Figure 5. For the Sublayer I and Jingmei Formation, the piezometric level of El. -3 m in 1999 is adopted in numerical analysis. The water pressures for sublayers II to IV are interpolated between sublayers V and I. Inside the pit, the piezometric levels maintaining at a depth of 1m below the excavation levels in each stage have been adopted in the analysis.

Proceedings DOI: 10.21467/proceedings.159
ISBN: 978-81-965621-6-8

Series: AIJR Proceedings
ISSN: 2582-3922

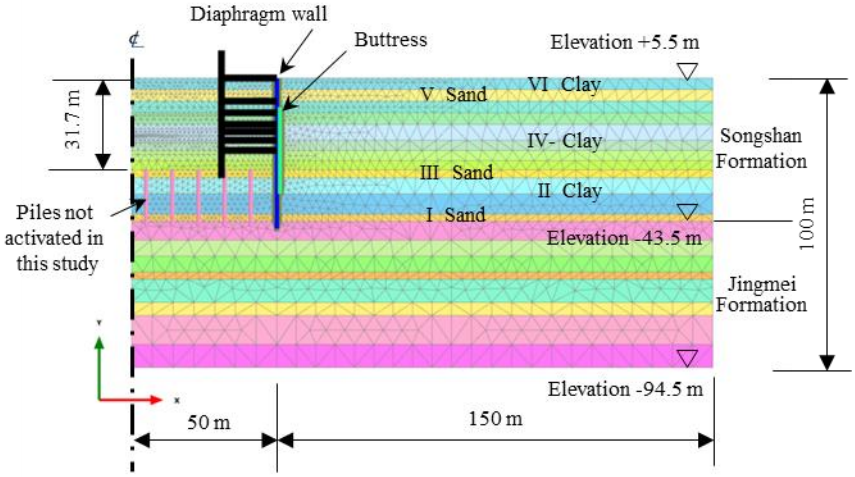

Figure 6: *Finite element mesh for the analytical section for 9 stages of excavation*

3 Numerical Simulation

3.1 Finite element mesh

The section analyzed is depicted in Figure 6. The excavation is carried out to a depth of 31.7 m in 9 stages in the analysis. While the CPC project site had the widths of 100 m and 118 m along the east-west and the north-south directions respectively, a half-width of 50 m has been adopted in the model. The diaphragm wall is located at a distance of 50 m from the axis of the trench. Because of symmetry in geometry, only half of the section has been analyzed as depicted in Figure 6. The lateral extent of the finite element model behind the diaphragm wall is 150 m, which is 4.7 times of the final excavation depth of 31.7 m. The Jingmei Formation underlying the Sungshan Formation is a water-rich gravelly stratum. This stratum is a competent formation with very high stiffness and is frequently assumed to be the base of the numerical analysis. Since there is presence of a sand and stiff clay stratum at the depths between 56 m and 82 m, the base of the finite element model in this study is placed at a depth of 100 m to include a 51 m layer of the Jingmei Formation to ensure that the contribution of this formation to ground movement is accounted for.

3.2 Nonlinearity of soil behavior - Hardening-soil with small-strain stiffness model

The PLAXIS-2D finite element software developed by PLAXIS BV (2013) has become a very popular tool in geotechnical analysis and design. The Hardening-Soil with Small-strain stiffness (HSS) constitutive soil model is an extension of the Hardening-Soil model (Schanz & Vermeer 1998; Benz Thomas, 2006; Schanz *et al.*, 1999) introduced in the PLAXIS program and is adopted herein to simulate the non-linear stress-strain relationship of soils under loading and unloading conditions. In the HSS model, the parameters adopted to define the hyperbolic stress-strain relationship are as follows:

- E^{ref}_{50} is the reference secant stiffness from standard triaxial drained test,
- E^{ref}_{oed} is the reference tangent stiffness for oedometer primary loading,
- E^{ref}_{ur} is the reference unloading-reloading stiffness from standard triaxial drained test,
- m is the exponential factor for stress-level dependency of stiffness,
- R_f is the failure ratio, $R_f = q_f / q_a$,
- q_a is the asymptotic value of the shear strength and q_f is the failure strength,
- G^{ref}_0 is the reference shear modulus at the level of very small strains,

- $\gamma_{0.7}$ is the reference shearing strain to define the behavior of degradation of moduli when G^{ref}_0 is reduced to 0.7 G^{ref}_0.

The stress-strain curves can be determined from laboratory tests such as the K_0-consolidated triaxial undrained compression and extension tests. In this study, the stiffness values of soils are related to the undrained shear strengths for clays and the N values for sands as expressed in the empirical Equations 2 to 6:

$$E^{ref}_{50} = 150\ s_u \text{ (for clayey soils)} \quad (2)$$

$$E^{ref}_{50} = 2\ N \text{ (in MPa for sandy soils)} \quad (3)$$

$$E^{ref}_{oed} = E^{ref}_{50} \quad (4)$$

$$E^{ref}_{ur} = 5\ E^{ref}_{50} \quad (5)$$

$$G^{ref}_0 = 1.07\ E^{ref}_{ur} \quad (6)$$

in which s_u is the undrained shear strengths of clayey soils and N is the blow-counts obtained in standard penetration tests for sandy soils. The parameters adopted in this study are summarized in Table 1. The empirical Equations (2) to (5) have been calibrated against a well-documented case history that Wong (2023) reported. The effective shear strength parameters, i.e., the c' and ϕ' values, for the silty sand strata, are determined from laboratory tests conducted on thin-wall tube specimens. For the clayey layers, c' = s_u and ϕ' = 0° is assumed in the analyses. The dilation angle, ψ', of 2°, 0°, and 3° are adopted for the sandy, the clayey, and the gravelly soils respectively. The R_f equals 0.9 is adopted. The unload-reload Poisson's ratio, υ_{ur}, of 0.2 is used as suggested by Benz Thomas (2006) and Schanz *et al.*, (1999). Although the HSS soil model is an effective stress model and adopting the ϕ' = 0° for the clayey soils loses its compression hardening function and stress-dependent stiffness, parametric studies using both the effective stress and the total stress models show that the computed wall deflections and surface settlements are essentially the same. The total stress input parameters for clay have been adopted in this study.

Table 1: *Soil parameters for the HSS model adopted in the PLAXIS analyses*

Mid depth m	Soil type	Unit weight γ' kN/m³	N value	Undrained shear strength s_u, kPa	Effective cohesion c' kPa	Effective friction angle ϕ', deg	Dilation angle ψ' deg	Reference stiffness		Initial shear moduli G^{ref}_0, MPa
								Secant stiffness E^{ref}_{50}, MPa	Unload-reload E^{ref}_{ur}, MPa	
2	CL	19	2	50				7.5	38	40
6	SM	19	8	-	0	32	2	16	80	86
9.75	CL	18.4	3	57				8.6	43	46
13.75	CL	18.4		60				9.0	45	48
18.75	CL	18.4		78				11.7	59	63
23	CL	19	7	98				14.8	74	79
26.5	CL	19		115				17.3	86	92
30.25	CL	19		133				20	100	107
33.25	SM	19.3	14	-	0	32	2	28	140	150
33.75	CL	19.5	14	169				25	127	136
44	CL	19.5	14	199				30	149	160
48.25	SM	20.3	35	-	0	32	2	70	350	375
52.75	GM	21.9	>100		0	35	3	200	1,000	1,070
61.5	CL/SM	19.5	25	-	0	32	2	50	250	268
68.25	SM	21.6	50	-	0	33	2	100	500	535
73.5	CL/SM	19.9	29	-	0	32	2	58	290	310
79.75	SM	19.7	50	-	0	33	2	100	500	535
91	GM	21.9	>100		0	35	3	200	1,000	1,338

Proceedings DOI: 10.21467/proceedings.159
ISBN: 978-81-965621-6-8

Series: AIJR Proceedings
ISSN: 2582-3922

3.3 Determination of small-strain stiffness

The parameters for the small-strain stiffness, i.e., the G^{ref}_0 and the $\gamma_{0.7}$, have been determined from the laboratory tests. Kung *et al.*, (2009) presented the results of small-strain triaxial tests and bender element tests conducted on undisturbed specimens recovered from clayey Sublayer IV of the Songshan Formation. The specimens were saturated and K_0-consolidated to the in-situ effective stress states. The K_0 values applied for consolidation ranged from 0.5 to 0.55. After completing the K_0-consolidation, but prior to the shearing tests, bender element tests were carried out to measure the shear moduli of the clay specimens. Compression and extension undrained triaxial shearing tests were then conducted. The undrained shear strengths profile obtained is presented in Figure 3. Based on the results of the bender element tests, Kung *et al.* (2009) obtained the G_{max}/s_u ratios ranging from 738 to 788, with an average ratio of 759 for the axial compression tests, where G_{max} is the initial shear modulus. For the axial extension tests, the G_{max}/s_u ratios ranged from 614 to 751, with an average of 671. In this study, the $G^{ref}_0 = 800\ s_u$ is adopted.

The reference shearing strain $\gamma_{0.7}$ value would range from 0.8×10^{-4} to 1×10^{-3}. Chin *et al.*, (2007) presents the stress-strain curve of a CK_0UDSS test conducted on Taipei clay. Wong (2023) reported the degradation of the shear moduli with shear strain interpreted from this direct simple shear test, showing that the Taipei clay would have the threshold $\gamma_{0.7}$ value of 5×10^{-4}. In this study, a $\gamma_{0.7}$ value of 6×10^{-4} is adopted.

3.4 Modeling of the retaining structures

In the numerical model, the diaphragm walls are modelled as plate elements. The E value of 25,000 MPa is adopted for concrete with a characteristic compressive strength, i.e. f'_c value, of 28 MPa. Following the normal practice to account for the influence of cracking, creep and relaxation of concrete during excavation, the flexural stiffness, EI, (I = moment of inertia) and the axial stiffness, EA (A = sectional area) values, of the diaphragm walls and the buttress are reduced by 30 %. The diaphragm wall and the buttress are essentially the flange and the web of an integrated T-section respectively. For a spacing of 8.75 m, the buttresses increase the EA by 11.30 GN/m and the EI values by 67.72 GNm^2/m. As shown in Figure 2, there were several buttresses on both sides of SID-2. The increase in the wall stiffnesses due to the buttresses spacing at 8.75 m can be fully accounted for. In consideration of the fact that SID-5 was 17.5 m away from the nearest buttress at the east wall and SID-7 was 8.75 m away at the south wall, a contribution factor, μ, of 25 % is applied to the former and 50 % to the latter due to the buttresses. Table 2 summarized the contribution factors adopted for the diaphragm walls and the buttresses located next to the inclinometers.

Table 2: *Cases studied in numerical analysis*

Case	Configuration of diaphragm wall, buttresses & inclinometer	Contribution factor, μ, %	Interface reduction, R_{inter}	Inclino -meter	Wall location	Excavation width, m
1	No buttress	0	0.52	SID-8	West	100
2	Inclinometer 17.5 m to buttress	25	0.6	SID-5	East	100
3	Inclinometer 8.75 m to buttress	50	0.8	SID-7	South	118
4	At centre of buttresses spaced 8.75 m	100	1	SID-2	North	118
5	At centre of buttresses spaced 4.38 m	200	1	-	-	118

3.5 Case analyzed

In order to study the effectiveness of the buttresses, 5 cases with the various buttresses spacing at various distances to the nearest panel have been analyzed. Case 1 has no buttress. Case 4 and Case 5 have the

buttress panels spacing at 8.75 m and at 4.38 m respectively. The inclinometers for Case 2 and Case 3 are located at 8.75 m and at 17.5 m to the nearest panel respectively. The stiffness values adopted for the flanges and the webs for these 5 cases are summarized in Table 3.

Figure 2 shows that inclinometers SID-1, SID-2 and SID-4 are located at the distances ranging from 17 m to 38 m to the corners of the basement excavation. The wall deflections observed in these 3 inclinometers are compared with those computed by the 2-Dimensional analysis for Case 4 to assess the corner effect.

The pit was braced by 7 levels of floor slabs, namely, the ground level floor (GF) and 6 basement floor (B1 to B6) slabs during excavation and by the base slab at the end. The floor slabs were 150 mm in thickness and are represented by fixed-end anchors in the analyses. Openings such as elevator shafts and staircases were provided on the floor slabs for de-mucking soils and for delivering construction materials and steel struts.

In addition to the concrete creeping effect, the axial stiffnesses of the B3 to B6 floor slabs have been further reduced by 0.59 to account for the effects of the openings. Beneath the spherical block that shown in Figure 1, there were the permanent circular openings of 35 m in diameter at the GF and B2 floor slabs. The 0.41 reduction factor is adopted for these 2 floors. At the B1 floor, the permanent opening was 60 m x 70 m. This wide opening was supported with temporary steel struts of twin H400x400x13x21 spacing at 8.75 m along both directions. The reinforced concrete slab for B1 occupied only 20 % of the floor area and the reduction factor of 0.20 is adopted. The combined reduction in the slab stiffnesses are summarized in Table 4.

Table 3: *Stiffnesses of diaphragm wall and buttress adopted in numerical analysis*

Case	Wall location	Flange element		Web element			Combined T-section	
		0.7EA GN/m	0.7EI GNm^2/m	Contribution factor, μ, %	0.7EA GN/m	0.7EI GNm^2/m	0.7EA GN/m	0.7EI GNm^2/m
1	West	26.355	4.94	0	0	0	26.36	4.94
2	East	26.355	4.94	25	2.82	16.93	29.18	21.87
3	South	26.355	4.94	50	5.65	33.86	32.01	38.80
4	North	26.355	4.94	100	11.30	67.72	37.65	72.66
5	-	26.355	4.94	200	22.59	135.44	48.95	140.38

Table 4: *Floor slab stiffnesses*

Floor level	Slab thickness mm	Axial stiffness AE, MN/m	Reduction factor			Input axial stiffness MN/m
			Creep	Opening	Combined	
GF, B2	150	3750	0.7	0.41	0.285	1070
B1	150	3750	0.7	0.20	0.14	530
B3 to B6	150	3750	0.7	0.59	0.41	1540

3.6 Modelling of soil-structure interface

The interface between the soil and the wall structure is a critical issue to be considered in soil-structural interaction analyses of deep excavations. In the PLAXIS software, an elastic-plastic model following the Mohr-Coulomb criterion is used to simulate the interaction effects between the walls and the soil. According to the Reference Manual (Bentley, 2022), the strength properties of the interface are related to the strength properties of a soil layer by a strength reduction factor, $R_{inter.}$ The interface is assumed to be rough with the full soil strength available with R_{inter} equals to 1. The stresses and strains developed along the soil-wall interface would be inversely proportional to the contact areas of the interface. In this

Proceedings DOI: 10.21467/proceedings.159
ISBN: 978-81-965621-6-8

Series: AIJR Proceedings
ISSN: 2582-3922

study, the roughness of the soil-wall interface has been proportional to L_t, the unit length of a typical T-section with the buttresses spacing at 8.75 m. Let L_1 denotes the distance between the inclinometer and the buttress and L_2 denotes the breadth of the buttress, the unit length of the soil-wall interface on the buttress side, L_i, is $(L_1+L_2)/L_1$. The L_i values for Case 1 to Case 4 are compared with the L_t value. Table 5 summarizes the L_i/L_t ratios for Case 1 to Case 4 ranging from 1 to 0.54. The R_{inter} values ranging from 0.52 to 1 have been adopted in this study.

Table 5: *Proportioning the strength reduction factors with the lengths of soil-wall interface*

Case	Distance of inclino-meter to buttress, L_1, m	Breadth of buttress, L_2, m	Unit length of soil-wall interface, m		Ratio L_i/L_t	R_{inter} adopted
			$L_i = (L_1+L_2)/L_1$	T-section, L_t		
1	4.38	0	1	1.85	0.54	0.52
2	17.5	3.7	1.21	1.85	0.65	0.6
3	8.75	3.7	1.42	1.85	0.77	0.8
4	4.38	3.7	1.85	1.85	1	1

4 Results Of Numerical Analysis

4.1 Computed wall deflections

Hwang *et al.* (2007) presented the wall deflection profiles observed at 6 inclinometers. The computed wall deflections for Case 1 and Case 2 in the final stage are presented in Figure 7. The matching between the computed maximum wall deflection, $\delta_{h\text{-}max}$, and that observed at SID-8 is close, with the difference of -1.5 mm for Case 1. For Case 2, the difference between the computed $\delta_{h\text{-}max}$ and that observed at SID-5 is 6.8 mm.

The computed wall deflections for Case 3 are presented in Figure 8, showing the consistence between the computed and the observed profiles in the various stages. The computed $\delta_{h\text{-}max}$ in the final stage of 149.7mm deviates from 154 mm that observed at SID-7 by 4.3 mm.

The computed $\delta_{h\text{-}max}$ values for Case 1 to Case 5 in the final stage are summarized in Table 6. The close matching between the computed and the observed wall deflections for Case 1 to Case 3 validates the R_{inter} values ranging from 0.52 to 0.8 adopted for these cases. The R_{inter} value of 0.52 for Case 1 would imply that the diaphragm wall without buttress could have a relatively smooth soil-wall interface. The $\delta_{h\text{-}max}$ values computed by the 2-dimensional analysis for Case 4 are 13 % to 44 % larger than those observed at inclinometers SID-1, SID-2 and SID-4, which are under the influence of the corner effect.

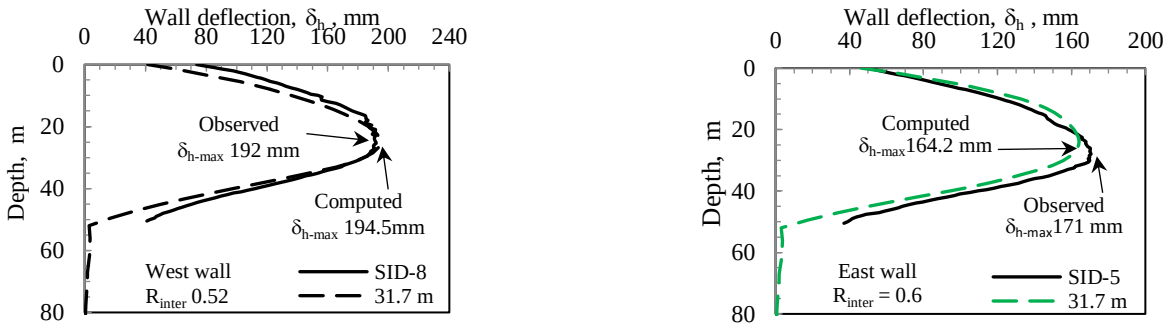

(a) West wall - Case 1

(b) East wall – Case 2

Figure 7: *Computed and observed wall deflections for east wall and west wall in final stage – Case 1 and Case 2*

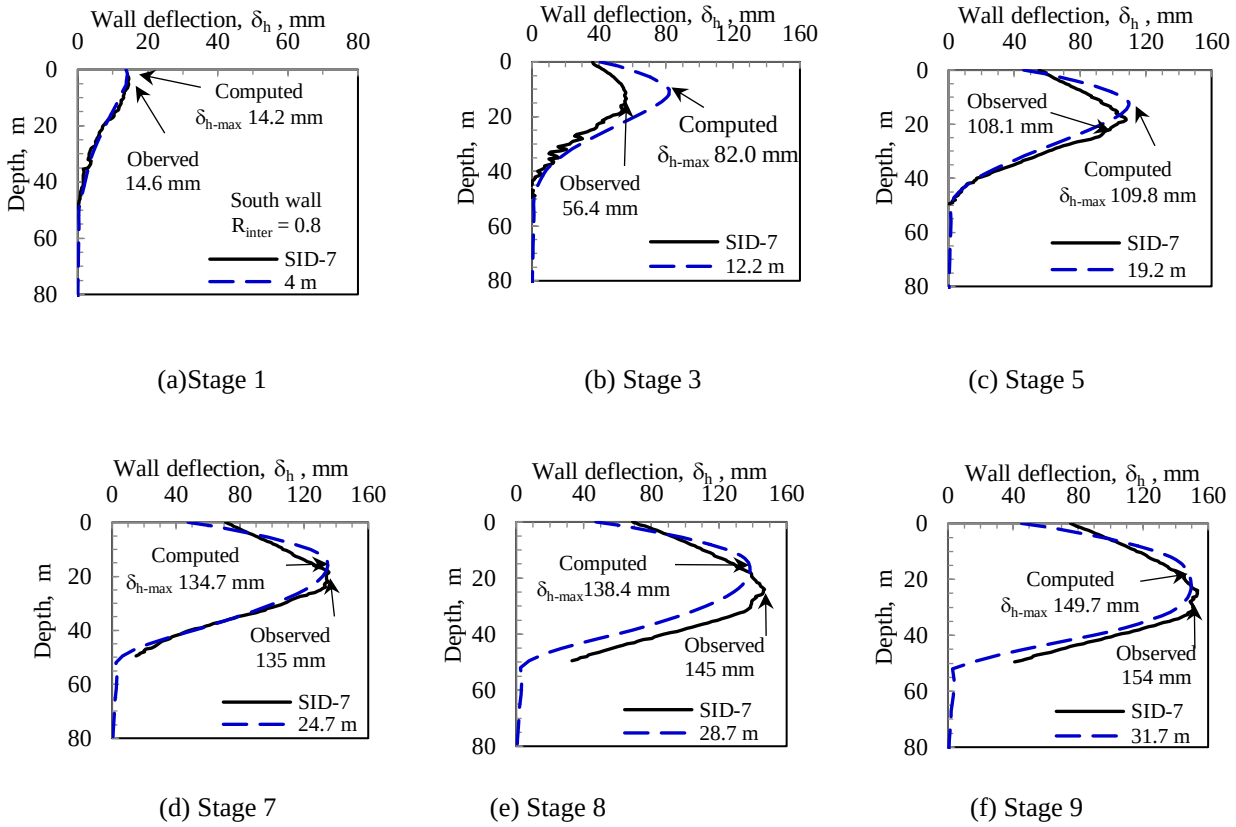

(a)Stage 1 (b) Stage 3 (c) Stage 5

(d) Stage 7 (e) Stage 8 (f) Stage 9

Figure 8: *Computed and observed wall deflections at south wall – Case 3*

Table 6: *Computed wall deflections for various cases in final stage*

Case	Analyzed section	Inclino -meter	Excavation width, m	Interface reduction, R_{inter}	Maximum wall deflection, $\delta_{h\text{-}max}$, mm		
					Observed	Computed	% difference
1	West	SID-8	100	0.52	192	194.5	1.3
2	East	SID-5	100	0.6	171	164.2	-4.0
3	South	SID-7	118	0.8	154	149.7	-2.8
4	North	SID-2	118	1	97	139.2	44
		SID-4	118	1	115	139.2	21
		SID-1	118	1	123	139.2	13
5	-	-	118	1	-	142.2	-

Proceedings DOI: 10.21467/proceedings.159
ISBN: 978-81-965621-6-8

Series: AIJR Proceedings
ISSN: 2582-3922

4.2 Effectiveness of buttresses

The computed wall deflections for Case 1 to Case 5 in the final stage are plotted in Figure 9 and summarized in Table 6. The family of deflection profiles shows that there is a trend of reduction in the radius of curvature of the wall at the buttress portion between the depths of 10.5 m and 40 m.

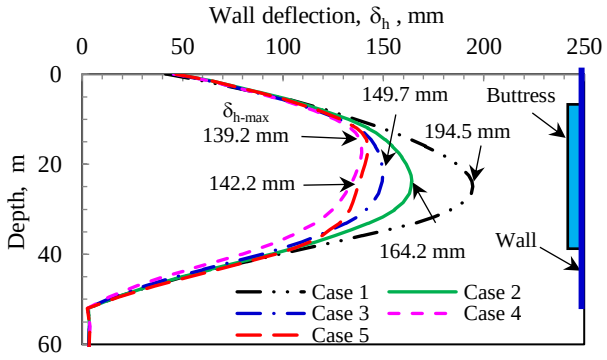

Figure 9: *Computed wall deflections with various wall stiffnesses at excavation depth 31.7 m*

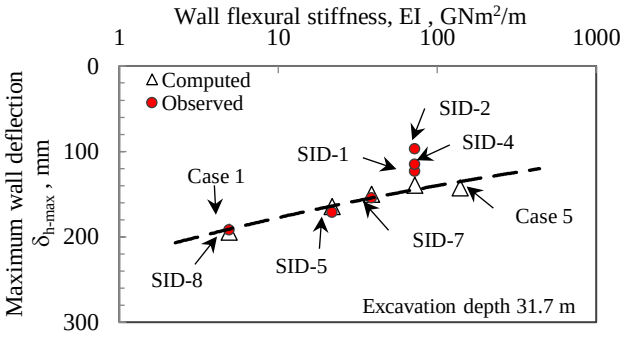

Figure 10: *Relationship between wall deflections and wall stiffnesses*

Figure 10 presents the variation in the $\delta_{h\text{-}max}$ values in the final stage with the various wall stiffnesses for Case 1 to Case 5, showing the trend of reduction in wall deflections with increase in wall stiffnesses. The computed maximum wall deflections for Case 1 to Case 3 agree with those observed. The $\delta_{h\text{-}max}$ values observed at SID-1, SID-2 and SID4, ranging from 97 m to 123 mm, are lower than the computed 139.2 mm for Case 4. The actual wall deflections at SID-1, SID-2 and SID4 being significantly lower than the trend line could be attributed to the corner effect.

4.3 Computed surface settlements

As depicted in Figure 2, the 4 settlement markers, S39, S40, S56 and S57 were located at the horizontal distances of 16 m to 52 m from the east wall. These markers were installed on the footings of the 4-storey buildings. The 6 settlement markers, S67 to S72, were installed on the ground surface at 2 m to 25 m from the south wall. Figure 11 presents the computed surface settlements behind the east wall for Case 2. Close matching between the analyzed and the observed settlements has been achieved in Stages 8 and 9. In Stage 9, the computed maximum settlement, $\delta_{v\text{-}max}$, of 136.2 mm is close to the observed 133 mm.

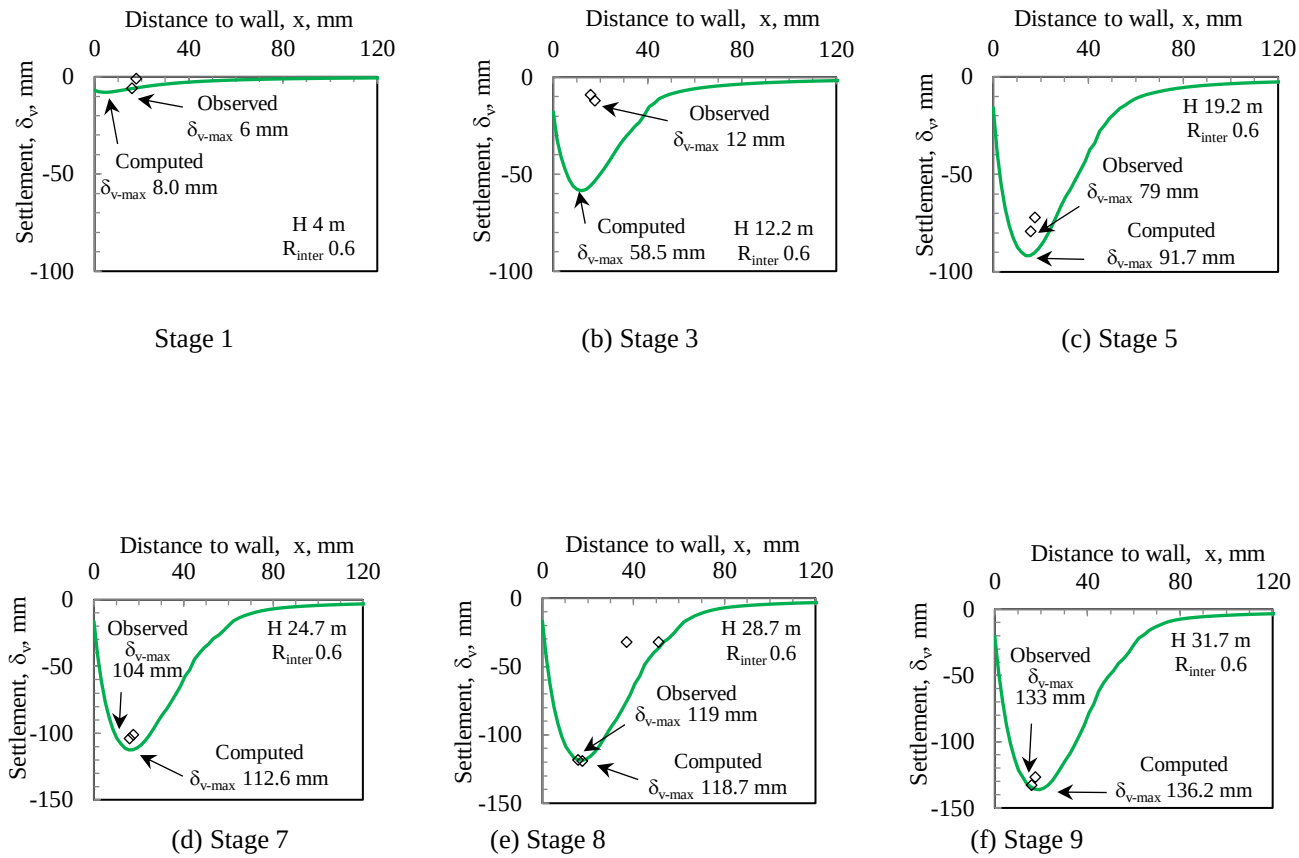

Figure 11: *Computed and observed surface settlements behind east wall – Case 2*

Figure 12 presents the computed δ_v values behind the south wall for Case 3. The observed settlements significantly exceed those computed in all stages. In Stage 9, the observed $\delta_{v\text{-}max}$ of 190 mm is 1.55 times of the computed value of 122.6 mm. With the observed $\delta_{h\text{-}max}$ of 154 mm at SID-7, the observed settlement to wall deflection ratio, $\delta_{v\text{-}max}/\delta_{h\text{-}max}$, is 1.23 on the south side. On the east side, the observed $\delta_{v\text{-}max}$ is 133 mm and the observed $\delta_{h\text{-}max}$ is 171 mm at SID-5 in the final stage, with the $\delta_{v\text{-}max}/\delta_{h\text{-}max}$ ratio of 0.78. On the south side, the $\delta_{v\text{-}max}/\delta_{h\text{-}max}$ ratio of 1.23 exceeding unity could be attributable to consolidation. Such consolidation effect to surface settlements is not modelled in this study.

Figure 1(a) shows that there is an underground railway aligned along the south side of the CPC project site. The distances of the railway tunnel to the south wall range from 15 m to 40 m. Hwang (2023) advised that the diaphragm wall for constructing the underground railway was approximately 40 m in length. The damming effect of that diaphragm wall blocked the seepage paths in the sandy Sublayers III and V. Groundwater recharging to the soil strata between the south wall and the railway tunnel via those 2 sandy sublayers was then disabled. Piezometers monitoring at 10 m horizontal distance behind the south wall showed that the piezometric level in Sublayer I was lowered from El. -4.2 m in January 1999 to El. -10.2 m in June 2000. The 6 m drawdown could contribute to the consolidation settlements.

Proceedings DOI: 10.21467/proceedings.159
ISBN: 978-81-965621-6-8

Series: AIJR Proceedings
ISSN: 2582-3922

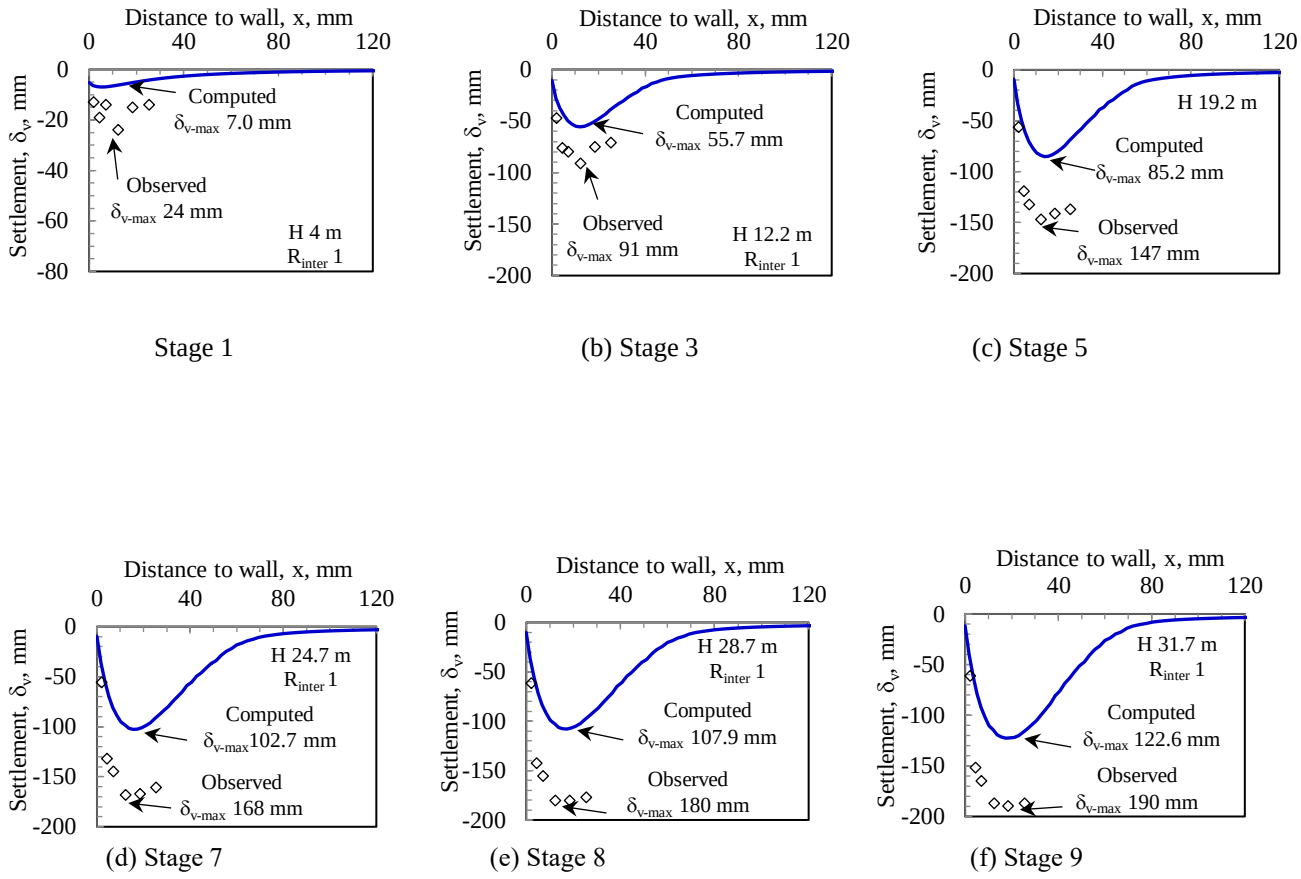

Figure 12: *Computed and observed surface settlements behind south wall – Case 3*

4.4 Normalized settlement profiles

Figure 13 presents the normalized computed and observed settlement profiles behind the south and the east walls in Stage 7 to Stage 9. The surface settlements, δ_v, are normalized with the maximum settlement, $\delta_{v\text{-}max}$ and the distances to the wall, the x values, are normalized with the excavation depth, H, of each stage. Although the observed settlements behind the south wall are far larger than those computed, the shapes of the normalized profiles match with those computed within 1H behind the wall. In Stage 8, the normalized observed settlement profile behind the east wall matches with that computed within the distance 2H. The matching between the observed and the computed normalized settlement profiles shows that the numerical analysis using the HSS model could reliably predict the magnitude and the shape the surface settlements.

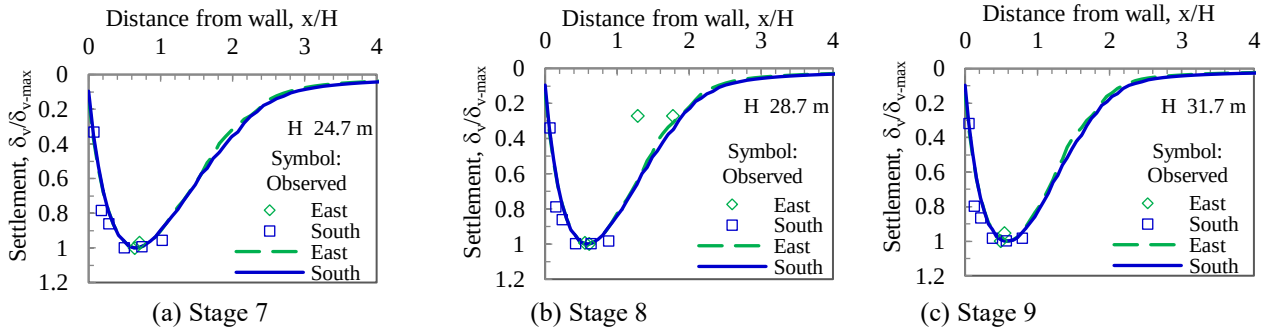

Figure 13: *Normalized computed and observed surface settlements behind the south and the east walls*

5 Conclusion

Two-dimensional numerical analysis on an excavation case history in soft ground has been conducted. The top-down construction for the maximum excavation depth of 31.7 m was supported by diaphragm wall with buttresses panels. The nonlinear Hardening-soil with small-strain stiffness (HSS) soil model is adopted. The following conclusions could be drawn:

(1) The HSS soil model could estimate the wall deflections and the surface settlements simultaneously.

(2) The presence of the buttress wall could affect the roughness along the soil-wall interface, which is one of the key parameters affecting the performance of wall deflections and surface settlements.

(3) The analysis confirms the trend of reduction in wall deflections with increasing in wall stiffnesses.

The set of the parameters for the small-strain stiffness adopted in this study has been interpreted from the laboratory tests and verified by an excavation case history. Close matching of the computed results with those observed in this case history further verifies the parameters.

6 Publisher's Note

AIJR remains neutral with regard to jurisdictional claims in institutional affiliations.

How to Cite

L.W. Wong (2023). Performance of Buttress Wall in a Deep Excavation in Soft Ground. *AIJR Proceedings*, 78-93. https://doi.org/10.21467/proceedings.159.8

References

Bentley. (2022). *PLAXIS CONNECT Edition V22.02 PLAXIS 3D-Reference Manual* (V22.02). Bentley Advancing Infrastructure.

Benz Thomas. (2006). *Small-Strain Stiffness of Soils and its Numerical Consequences* [The Institute of Geotechnics]. https://d-nb.info/984776931/04

Chen, Y.K, Huang, C.C & Wang, F.G. (1997). Grouted raft for building protection in excavation in soft clay. Proc.,7th Conf. on Current Research in Geotechnical Engineering, Taiwan, Vol. 1:593-600. (in Chinese)

Chin, C. T., Chen, J. R., Hu, I. C., Yao, D. H. C., & Chao, H. C. (2007). Engineering characteristics of Taipei clay. In T. S. Tan, K. K. Phoon, D. W. Hight, & S. Leroueil (Eds.), *Characterization and Engineering Properties of Natural Soils* (1st ed., pp. 1755–1803). Taylor & Francis Group. https://doi.org/10.1201/NOE0415426916

Chin, C. T., Crooks, J. H. A., & Moh, Z. C. (1994). Geotechnical properties of the cohesive Sungshan deposits,Taipei. *Geotechnical Engineering*, 77–103. http://seags.ait.asia/e-journal/1970-2012/GEJ_1994_v25n2_December.pdf

Chin, C.T. & Liu, C-C. (1997). Volumetric and undrained behaviors of Taipei silty clay. J. Chinese Institute of Civil and Hydraulic Engineering, Taipei, Taiwan 9(4): 665-678. (in Chinese)

Chuang, M.H., Chou, C.R., Su, T.C. & Wang, C.H. (2002). A case study of 32 m excavation in soft ground. Proc., Urban Underground Construction and Environmental Protection, Cross-Strait Geotechnical Conference, Shanghai, China. 171-180. (in Chinese)

Hu. I.C., Chin, C. T., & Liu, C. J. (1996). *Review of the Geotechnical Characteristics of the Taipei Basin*. https://www-geotech-org-tw.translate.goog/purchase-inner.php?id=134&_x_tr_sl=zh-TW&_x_tr_tl=en&_x_tr_hl=en&_x_tr_pto=sc&_x_tr_sch=http

Hwang, R. (2023). Personal communication.

Hwang, R. & Moh, Z.C. (2022). Groundwater drawdown and subsidence in the Taipei Basin. Sino-Geotechnics, No. 173/2022.9: 99-110. (in Chinese) http://www.geotech.org.tw/purchase-inner.php?id=202

Hwang, R. N., Moh, Z.-C., & Wang, C. H. (2007). Performance Of Wall Systems During Excavation for Core Pacific City. *Journal of GeoEngineering*, *2*(2), 53–61. http://yo-1.ct.ntust.edu.tw/jge/files/articlefiles/v2i2200709052124061480.pdf

Kung, G. T. C., Ou, C. Y., & Juang, C. H. (2009). Modeling small-strain behavior of Taipei clays for finite element analysis of braced excavations. *Computers and Geotechnics*, *36*(1–2), 304–319. https://doi.org/10.1016/J.COMPGEO.2008.01.007

Lee, S.H. (1996). Engineering geological zonation for the Taipei City. Sino-Geotechnics, (54): 25-34. (in Chinese)

MAA (1987) Engineering properties of the soil deposits in the Taipei Basin, Report No. 85043, Ret-Ser Engineering Agency and Taipei Public Works Department, Taipei. (in Chinese)

MOH, Z. C., & OU, C. D. (1979). Engineering characteristics of Taipei Silt. *Sixth Asian Regional Conference on Soil Mechanics and Foundation Engineering*, 155–158. http://www.maaconsultants.com/common/publications/1976/1976-014.pdf

Ou, C.Y., Liao, J.T. & Cheng, W.L. (2000), Building response and ground movements induced by a deep excavation, Geotechnique, Vol. 50, No. 3: 209-220.

Ou, C. Y., Lin, Y. L., & Hsieh, P. G. (2006). Case Record of an Excavation with Cross Walls and Buttress Walls. *Journal of GeoEngineering*, *1*(2), 63–73. https://doi.org/10.6310/JOG.2006.1(2).4

PLAXIS B.V. (2013). PLAXIS Reference Manual. PLAXIS, BV, Delft, the Netherlands.

Schanz, T. & Vermeer, P.A. (1998). On the Stiffness of Sands. Geotechnique, 46, No. 1: 145-151.

Schanz, T., Vermeer, P. A., & Bonnier, P. G. (1999). The hardening soil model: Formulation and verification. In *Beyond 2000 in computational geotechnics. Ten Years of PLAXIS International. Proceedings of the international symposium, Amsterdam, March 1999.* (pp. 281–296). A.A.Balkema. https://doi.org/10.1201/9781315138206-27

Wong, L. W. (2023). Effects of soil-structure interaction on wall deflections and surface settlements during deep excavations. *Towards a Smart-Green-Resilient Geo-Future for World-Class City Development Proceedings of the 43rd Annual Seminar*, 70–81. https://firebasestorage.googleapis.com/v0/b/hkieged-org.appspot.com/o/public%2F1684999119243.pdf?alt=media&token=4d23de79-65f9-4e57-85e5-d937d3368aa8